

Tropical Tropospheric Temperature and Precipitation Response to Sea Surface Temperature Forcing

Hui Su and J. David Neelin

*Department of Atmospheric Sciences, and Institute of Geophysics and Planetary Physics,
University of California, Los Angeles, Los Angeles, California*

Joyce E. Meyerson

Department of Atmospheric Sciences, University of California, Los Angeles, Los Angeles, California

During an El Niño event, there are substantial tropospheric temperature anomalies across the tropics associated with sea surface temperature (SST) warming in the central and eastern Pacific. The typical spatial scale for teleconnection response of tropospheric temperature tends to be large. On the other hand, the precipitation response exhibits strong compensation between positive response over warm SST anomalies and a complex negative response remotely. The tropical spatial averages of tropospheric temperature and precipitation thus yield an interesting contrast in behavior. Anomalies of tropical averaged precipitation for 3-month averages appear quite scattered in relation to tropical SST anomalies, while the tropical mean tropospheric temperature obeys an approximately linear relationship to SST. This different behavior of tropical mean precipitation and tropospheric temperature in relation to SST is examined in detail using observational data, GCM simulations and idealized experiments with the quasi-equilibrium tropical circulation model (QTCM). Theoretical understanding is provided through a simple analytical model, which suggests that the integral constraint on tropical average precipitation is dominated by dry static energy transport into or out of the tropics. Convection acts to keep tropospheric temperature in quasi-equilibrium (QE) with boundary layer moist static energy, which is in turn held toward SST by surface fluxes. To maintain QE, the tropical average convective heating (i.e., precipitation) anomalies react to oppose any processes that tend to cool the tropical troposphere. Thus, while tropical average tropospheric temperature is closely related to SST, unrelated heating or cooling anomalies such as those due to the tropical-midlatitude transports can create large scatter in tropical average precipitation anomalies.

1. INTRODUCTION

1.1. Background

On interannual time scales, variability of tropical tropospheric-averaged temperature is dominated by El Niño/Southern Oscillation (Horel and Wallace 1981; Pan and Oort 1983; Sun and Oort 1995). When sea surface temperature (SST) is warmer than normal in the eastern and central Pacific, warm tropospheric temperature anomalies are observed across the entire tropical band (Yulaeva and Wallace 1994; Wallace et al. 1998). At the same time, substantial precipitation anomalies occur within the tropics. Unlike wide-spread tropospheric temperature warming, precipitation anomalies exhibit strong spatial variations. The spatial scale for teleconnection of tropospheric temperature (and associated wind vectors) appears larger than that for precipitation (Wallace et al. 1998; Su et al. 2001). In regions of warm SST anomalies, the amount of precipitation is increased. Away from the directly heated regions, precipitation is reduced, which is primarily a remote response to the warmest SST anomalies (Su et al. 2001). When the tropical average is considered, the near-cancellation of positive and negative precipitation anomalies yields scattered tropical-mean precipitation anomalies $\langle P' \rangle$ in relation to tropical SST anomalies $\langle T'_s \rangle$. However, the tropical mean tropospheric temperature anomalies $\langle \hat{T}' \rangle$ are approximately linearly related to SST anomalies.

The approximately linear relationship of $\langle \hat{T}' \rangle$ to $\langle T'_s \rangle$ is examined in detail in Su et al. (2003, hereafter SNM). The scatter of $\langle P' \rangle$ with respect to $\langle T'_s \rangle$ is presented in Su and Neelin (2003, hereafter SN03). Here, we combine the results from SNM and SN03 to provide an overview of tropical tropospheric temperature and precipitation response to SST forcing on interannual time scales. The different characteristics of tropical tropospheric temperature and precipitation in relation to SST are compared using a variety of observational data and model results. Subsequently, with a simple analytical model we aim to examine the physical processes involved quantitatively, and thus gain insight into the dynamics governing the behavior of tropospheric temperature and precipitation response to interannual SST forcing. For present purposes, ENSO SST anomalies are discussed as a forcing to the atmosphere, and model simulations with specified SST are used. We focus on the simultaneous relationship of atmospheric variables to SST at 3-month averages, noting the caveat that for some phenomena ocean-atmosphere coupling needs to be considered.

The structure of this article is as follows: In section 1.2, the $\langle \hat{T}' \rangle$ and $\langle T'_s \rangle$ relationship is shown. The $\langle P' \rangle$ and $\langle T'_s \rangle$ relation is then presented in section 1.3. Section 2 provides additional cases for the relationship of $\langle \hat{T}' \rangle$, $\langle P' \rangle$ and $\langle T'_s \rangle$ using numerical model results. An analytical model is introduced in section 3 to unravel the approximately linear $\langle \hat{T}' \rangle$ but scattered $\langle P' \rangle$ with respect to $\langle T'_s \rangle$. In section 4, the dynamics for the $\langle \hat{T}' \rangle$, $\langle P' \rangle$ and $\langle T'_s \rangle$ relationship are described. Finally, conclusion and discussion are given in section 5.

1.2. The approximately linear relationship of $\langle \hat{T}' \rangle$ and $\langle T'_s \rangle$

The linear relationship between tropical mean tropospheric temperature and SST anomalies has been documented extensively (e.g. Newell and Weare 1976; Angell 1981; Horel and Wallace 1981; Pan and Oort 1983; Soden 2000; Kumar and Hoerling 2003), although many have used 200 hpa geopotential height or temperature as a proxy for tropospheric averaged temperature. Sobel et al. (2002) showed that interannual anomalies of tropical tropospheric temperature are correlated not only with SST anomalies averaged over the precipitating regions, but also with SST anomalies averaged over the entire tropics. In Fig. 1a, the tropical averaged (25 S-25 N) tropospheric (850-200 hpa) temperature anomalies are plotted against observed tropical SST anomalies (Reynolds and Smith 1994). Three temperature datasets are used, one of which is the NCEP/NCAR (National Center for Environmental Prediction (NCEP)/National Center for Atmospheric Research (NCAR)) reanalysis data from 1982 to 1998 (Kalnay et al. 1996). Another dataset consists of the satellite measurement (1982-1993) from the microwave sounding unit (MSU) associated with the vertical weighting functions of Channel 2-3 (Spencer and Christy 1992). The third is from a simulation with the quasi-equilibrium tropical circulation model (QTCM, Neelin and Zeng 2000) driven by observed SST anomalies from 1982-1998. A similar scatterplot using tropical averaged temperature at 200 hpa is shown in Soden (2000) Fig. 5c. It is clear that there is an approximate linearity between $\langle \hat{T}' \rangle$ and $\langle T'_s \rangle$ for the NCEP/NCAR reanalysis and MSU estimate. The QTCM simulation with observed SST also shows a prominent linear relationship. The slopes of the linear fits to each dataset are surprisingly close, all around $1.4 \text{ C } C^{-1}$. The model results have less scatter than the observed datasets due to reduced internal variability.

1.3. The scatter of $\langle P' \rangle$ in relation to $\langle T'_s \rangle$

Tropical mean precipitation anomalies, on the other hand, appear rather scattered with SST anomalies, as shown in Fig. 1b for four datasets. Besides the NCEP/NCAR reanalysis and the QTCM simulation driven by observed SST from 1982-1998, two combined satellite and rain gauge measurements of precipitation are used. One is from the Global Precipita-

tion Climatology Project (GPCP, Huffman et al. 1997) and the other is from the the Climate Prediction Center (CPC) Merged Analysis of Precipitation (CMAP, Xie and Arkin 1997). These two satellite products use similar satellite infrared, microwave emission and in-situ rain-gauge measurements, but with different algorithms. The MSU precipitation (Spencer 1993) used in Soden (2000) covers oceanic regions only, and thus is not displayed in Fig. 1b. The monthly precipitation anomalies are smoothed by a 3-month running mean, a typical filter for examining interannual anomalies. It is clear that tropical mean precipitation anomalies appear scattered with respect to tropical SST anomalies for all datasets. There is no simple relation between $\langle P' \rangle$ and $\langle T'_s \rangle$. Linear fits to the datasets show a wide range of slopes, with even negative slope for the CMAP precipitation. Defining P'_i and P_{Li}' as actual and linearly fitted precipitation anomalies at month i , respectively, the root-mean-square errors of the linear fits $(\frac{1}{N} \sum_{i=1}^N (P'_i - P_{Li}')^2)^{1/2}$ are comparable to the standard deviations of the datasets themselves, suggesting the linear fits are not representative of the relationship between $\langle P' \rangle$ and $\langle T'_s \rangle$. Similar scatter of $\langle P' \rangle$ versus $\langle T'_s \rangle$ is also found for a recent satellite product, the Tropical Rainfall Measuring Mission (TRMM) precipitation, although the temporal coverage of the TRMM data is much shorter (available since January 1998). The linear fit to the TRMM precipitation also gives a negative slope of $-0.2 \text{ mm day}^{-1} \text{ C}^{-1}$ (SN03). The linear correlations between $\langle P' \rangle$ and $\langle T'_s \rangle$ are 0.01 for the NCEP/NCAR reanalysis and the GPCP data, 0.21 for the QTCM result and -0.38 for the CMAP.

For a given tropical mean SST anomaly, the tropical mean precipitation anomaly could be of either sign. For example, the $\langle T'_s \rangle$ is about 0.4 C for September to November 1997, and 0.6 C for December 1997 to February 1998. The corresponding $\langle P' \rangle$ from the GPCP data is -0.2 mm day^{-1} for SON and 0.05 mm day^{-1} for DJF. Furthermore, the opposite signs of $\langle P' \rangle$ are associated with rather similar spatial distributions of precipitation anomalies as in Fig. 2. By viewing the horizontal maps alone, one cannot predict the sign of the tropical mean precipitation anomaly because of the near-cancellation of positive anomalies against negative anomalies.

The approximately linear relation between $\langle \hat{T}' \rangle$ and $\langle T'_s \rangle$ and the poor correlation between $\langle P' \rangle$ and $\langle T'_s \rangle$ on the interannual time scales seem contradictory to global warming scenario simulations where tropical mean precipitation increases as tropical mean SST increases (Mitchell et al. 1987; Dai et al. 2001). It also seems contradictory to a traditional view that increased SST enhances convective activity, and thus increases the precipitation rate and intensifies the hydrological cycle in the tropics (Holton 1992). For local precipitation anomalies near warm SST anomalies, the traditional theory holds (Ropelewski and Halpert 1987; Kiladis

and Diaz 1989). Thus it is of interest to understand why it fails in the tropical means on interannual time scales.

Soden (2000) pointed out that the performance of existing climate models in simulating the interannual variations of tropical mean tropospheric temperature is better than the performance in simulating the tropical mean precipitation variations. He attributed this discrepancy to two possible sources. One is the error of satellite measurements of tropical mean precipitation. The other is associated with problems of various physical parameterization schemes employed in climate models.

We concur with Soden that both observational data and numerical models might require improvement. However, the drastically different behaviors of $\langle \hat{T}' \rangle$ versus $\langle T'_s \rangle$ and $\langle P' \rangle$ versus $\langle T'_s \rangle$ (Fig. 1), and the difference in the performance of climate models in simulating the interannual variability of $\langle \hat{T}' \rangle$ and $\langle P' \rangle$ suggest that the dynamics governing the temperature and precipitation response to SST forcing may be fundamentally different. While SNM showed that tropical mean tropospheric temperature has a rather simple relationship with SST, Su and Neelin (2002) found the mechanisms for anomalous subsidence forced by ENSO warm SST anomalies involve a complex set of pathways. These involve feedbacks dependent on local climatology, and tend to vary among regions and events, although many share a unifying theme, namely, they are initiated by the temperature response. Thus, it is not surprising that GCMs are able to capture tropospheric temperature response but have more difficulty reproducing precipitation response.

2. ADDITIONAL CASES OF THE RELATIONSHIP OF $\langle \hat{T}' \rangle$, $\langle P' \rangle$ AND $\langle T'_s \rangle$

The precipitation data shown in Fig. 1b exhibit a wide range of linear correlation with $\langle T'_s \rangle$. The differences in the $\langle P' \rangle$ and $\langle T'_s \rangle$ relation for the observational data could potentially be due to errors in the satellite retrieval algorithms. Because observational data lack constraints in the moisture budget, the tropical mean precipitation values may be inconsistent with mass conservation. Hence, we extend our analysis to atmospheric model results that have a consistent moisture budget. First, we examine ensemble simulations from the National Aeronautics and Space Administration (NASA) Seasonal-to-Interannual Prediction Project (NSIPP) atmospheric GCM (Bacmeister et al. 2000; Pegion et al. 2000).

2.1. NSIPP experiments

Five NSIPP GCM simulations with different initial conditions are used. They are all driven by observed SST from 1930 to present. Only the results from 1982 to 1998 are shown for comparison to other datasets. Figure 3a shows the

scatterplot of $\langle P' \rangle$ versus $\langle T'_s \rangle$ for all five runs where both $\langle P' \rangle$ and $\langle T'_s \rangle$ are smoothed by a 3-month running mean. It is evident that the tropical mean precipitation anomalies have a large degree of variability and poor correlation with tropical average SST anomalies for all runs. The standard deviations of $\langle P' \rangle$ for individual runs are around $0.05 \text{ mm day}^{-1} \text{C}^{-1}$. A linear fit to all values of $\langle P' \rangle$ is shown by the dashed line, with a positive slope of $0.07 \text{ mm day}^{-1} \text{C}^{-1}$. The slopes of linear fits to individual runs range from 0.05 to $0.08 \text{ mm day}^{-1} \text{C}^{-1}$. However, the r.m.s. errors of the linear fits are very close to the standard deviations of $\langle P' \rangle$. Thus, a linear fit to $\langle T'_s \rangle$ explains little of the $\langle P' \rangle$ behavior as the linear correlation of $\langle P' \rangle$ to $\langle T'_s \rangle$ is only 0.01.

In contrast, the tropical averaged tropospheric temperature anomalies are strikingly linear with respect to the tropical mean SST forcing. Figure 3b shows the scatterplot of $\langle \hat{T}' \rangle$ versus $\langle T'_s \rangle$ for the five AGCM experiments. The approximate linearity is prominent, with a relatively large departure from linearity occurring at large warm SST anomalies. The slope of the linear fit to all data is about 1.76 CC^{-1} , which is slightly higher than values obtained from observational estimates of $\langle \hat{T}' \rangle$, approximately 1.4 CC^{-1} (Fig. 1a). The correlation of $\langle \hat{T}' \rangle$ to $\langle T'_s \rangle$ is 0.91 in Fig. 3b. The corresponding correlations of $\langle \hat{T}' \rangle$ to $\langle T'_s \rangle$ from the MSU and the NCEP/NCAR reanalysis are 0.80 and 0.77, respectively.

2.2. QTCM regional SST anomaly experiments

Besides analyzing the GCM results, we conduct idealized experiments with the intermediate climate model–QTCM (Neelin and Zeng 2000; Zeng et al. 2000). In this set of experiments, positive SST anomalies are specified over particular regions of the Pacific, while the rest of oceanic model domain uses climatological SST. The SST anomalies are of various shapes, areas, amplitudes and locations, although all are based on observed SST anomalies during JFM 1998 El Niño in some way. About 40 experiments are conducted, and each of them is an ensemble of 3-10 members with slightly different initial conditions. The spatial averages of tropospheric (850-200 hpa) temperature over the tropical band (25S - 25N) from the QTCM simulations are displayed as a function of SST forcing for the 40 experiments shown in Fig. 4a. The side panels show the simulated tropospheric temperature anomalies for different SST forcings, indicated by the heavy outlines. The panel on the right margin shows the distribution of positive SST anomalies observed during JFM 1998, with outlines indicating areas for regional SST forcings used in the four side panels. The ordinate of Fig. 4a is the *spatial integral* of the SST anomaly. It can be seen that there is a remarkable degree of linearity between the tropical mean tropospheric temperature and SST anomalies, despite the large range of regional size and spatial patterns sampled.

On the other hand, tropical mean precipitation anomalies bear no simple relation to SST forcing, nor to the tropospheric temperature anomaly, as shown in Fig. 4b. The intra-ensemble standard deviations for $\langle P' \rangle$ are 0.002 to 0.01 mm day^{-1} , depending on the ensemble size. Examples of the spatial distribution of precipitation anomalies are shown in side panels, corresponding to those in Fig. 4a. While the spatial patterns are qualitatively similar, the tropical average is set by the sum of positive anomalies local to the SST forcing, against weaker negative anomalies that may occur over a larger area. The near-cancellation can produce either sign in the tropical average.

In terms of spatial distribution of anomalies, the horizontal maps of tropospheric anomalies tend to be similar regardless of the configuration of SST forcing (Fig. 4a). The spatial pattern generally resembles the traditional wave response to a localized heat source, although with large longitudinal extent compared to heavily damped simple models (Gill 1980). In subregional SST anomaly runs (e.g. the upper and lower left panels in Fig. 4a), although positive SST anomalies are highly localized, the tropospheric temperature anomalies display broad warming in the whole tropical band. The scope of the warming in both zonal and meridional directions is similar to that for the run with the entire tropical Pacific positive SST anomaly (the upper right panel), indicating the effectiveness of wave dynamics in transporting the heating anomalies. On the other hand, the direct, positive response of precipitation to a positive SST anomaly is much more local and tends to be surrounded by negative anomalies. Although there exist negative precipitation anomalies in far-field, the amplitude is very weak. The tropical averaged precipitation is thus a sum of large positive values in a localized region and weak negative values over a broad area, leaving room for nonlinearity to complicate the response.

Because the scatter in tropical mean precipitation anomalies is common in all datasets and model simulations, it appears that this is not an artifact of observational error or imperfect numerical models. We conjecture that it is an inherent feature of the moist convective response to tropical SST forcing and other factors. In the next section, a simple model based on the equations of the QTCM (Neelin and Zeng 2000) is used to illustrate the dynamics governing the tropical mean precipitation and temperature variations.

3. ANALYTICAL CONSIDERATIONS FOR THE RELATIONSHIP OF $\langle T' \rangle$, $\langle P' \rangle$ AND $\langle T'_S \rangle$

3.1. Derivations

Following SN03, $\langle \hat{T}' \rangle$ and $\langle P' \rangle$ solutions can be derived for a steady-state atmospheric response to SST and mid-latitude forcing. We write the column-averaged temperature and

moisture perturbation equations as:

$$D_T' = \hat{Q}'_c + F_{rad}' + H' \quad (3.1)$$

$$-D_q' = \hat{Q}'_q + E', \quad (2)$$

where D_T and $-D_q$ are the horizontal divergences of the vertically-integrated dry static energy and moisture transports by the dynamics. The signs are chosen because the two tend to cancel on the tropical average. Using $\langle \rangle$ to denote the averages over the whole tropical band, we define $F_T' \equiv \langle D_T' \rangle$ and $F_q' \equiv \langle D_q' \rangle$, where F_T' and F_q' are the anomalous dry static energy and moisture fluxes across the boundaries (25S-25N) between the tropics and mid-latitudes, respectively. Positive values of F_T' imply an export of energy out of the tropics, while for F_q' , export of moisture out of the tropics corresponds to negative values. The anomalous moist static energy transport from the tropics, given by $F_T' - F_q'$, is usually less than the individual terms. The atmospheric column radiative heating rate is denoted as F_{rad} . The surface sensible and latent heat fluxes are H and E . The column-averaged convective heating and moisture sink are \hat{Q}_c and \hat{Q}_q , respectively, and they satisfy

$$-\hat{Q}_q = \hat{Q}_c = P \quad (3)$$

where $\hat{(\)}$ denotes vertical averaging over the troposphere and P is the precipitation rate. The $(\)'$ indicates perturbations relative to climatological means. All quantities are presented in energy units.

Combining (3.1) and (2), we obtain the moist static energy perturbation equation

$$F_{rad}' + H' + E' = D_T' - D_q'. \quad (4)$$

Similar to SNM, the flux balance can be approximated as linear functions of atmospheric temperature, moisture and SST. For simplicity, we neglect sensible heat flux anomalies because they are relatively small compared to latent heat flux anomalies. The coefficient for radiative flux anomalies due to atmospheric moisture changes can be combined with that for temperature changes because the tropical mean moisture anomalies can be approximately linearly fitted to tropospheric temperature anomalies. So we use only one proportionality parameter ϵ_T here. The evaporation anomalies are parameterized using the conventional bulk-aerodynamic formula. The evaporation anomaly due to changes in wind speed is not easily linearized, so it is denoted as \tilde{E} . All other nonlinear effects in the fluxes can be incorporated into \tilde{E} . The cloud-radiative forcing amounts to roughly 10% of the surface heat flux forcing and is omitted here. Thus, we have

$$-\epsilon_T \hat{T}' + \epsilon_{T_s} T_s' + \epsilon_H (\gamma T_s' - q_a') + \tilde{E} = D_T' - D_q'. \quad (5)$$

In (5), \hat{T}' represents the tropospheric temperature anomalies and T_s and q_a are sea surface temperature and near-surface air moisture (in units of K). The constants ϵ_T and ϵ_{T_s} are proportionality coefficients for the atmospheric radiative heating rate dependence on temperature and SST anomalies, with $\epsilon_T \approx 6 \text{ W m}^{-2} \text{ K}^{-1}$ and $\epsilon_{T_s} \approx 6 \text{ W m}^{-2} \text{ K}^{-1}$. We use $\epsilon_H = \rho_a C_H V_s$, where ρ_a is surface air density and C_H is the drag coefficient. The surface wind speed is denoted as V_s . For a tropical mean wind speed of 5 m s^{-1} , the value of ϵ_H is about $5 \text{ W m}^{-2} \text{ K}^{-1}$. The surface saturation moisture q_{sat} is a function of SST, with the dependence of $\gamma = \left(\frac{d q_{\text{sat}}}{dT} \right)_{T_s}$. Because the value of γ is nearly constant in the normal range of observed SST variations, we use $\gamma \approx 3 \text{ K K}^{-1}$, corresponding to an SST of 300 K.

When the tropical average of equation (5) is considered, the tropical mean moisture change can be related to the tropical mean tropospheric temperature variations due to the constraint on large-scale circulation by deep convection. In other words, convection vigorously adjusts tropospheric temperature to a value set by boundary layer moist static energy, which is largely determined by surface air moisture. Outside the region of deep convection, tropospheric temperature is not strongly tied to boundary layer moisture. However, the fraction of non-precipitating regions in the tropics is not large, so we try the approximation $\langle q'_a \rangle \approx \gamma n \langle \hat{T}' \rangle + \xi$ and fit it against model output. The perturbation term ξ indicates the contribution to tropical average moisture change not directly related to tropospheric temperature change, such as that over the non-precipitating regions. Its effect can be incorporated into \tilde{E} in (5), so it is omitted hereafter. The parameter n is a scale factor, considering the boundary layer sub-saturation and the ratio of surface air temperature to the tropospheric average temperature. The value of γn is 1.73 for the NSIPP model results, based on the linear regression of $\langle q'_a \rangle$ to $\langle \hat{T}' \rangle$ for the period of 1982 to 1998.

3.2. Analytical relationship of $\langle T' \rangle$, $\langle P' \rangle$ and $\langle T'_s \rangle$

Taking the tropical average of (5) and rearranging it, SN03 obtained the relationship between tropical average tropospheric temperature and SST anomalies

$$\begin{aligned} \langle \hat{T}' \rangle = & [(\epsilon_{T_s} + \epsilon_H \gamma) \langle T'_s \rangle - F_{T'} + F_{q'} + \langle \tilde{E} \rangle] \\ & \times (\epsilon_T + \epsilon_H \gamma n)^{-1}. \quad (6) \end{aligned}$$

Substituting (6) into (3.1) or (2), the $\langle P' \rangle$ and $\langle T'_s \rangle$ relation can thus be expressed as

$$\begin{aligned} \langle P' \rangle = & [\epsilon_H \gamma (\epsilon_T - n \epsilon_{T_s}) \langle T'_s \rangle + (\epsilon_H \gamma n) F_{T'} + \epsilon_T F_{q'} \\ & + \epsilon_T \langle \tilde{E} \rangle] (\epsilon_T + \epsilon_H \gamma n)^{-1}. \quad (7) \end{aligned}$$

Comparing (6) and (7), we notice that both $\langle \hat{T}' \rangle$ and $\langle P' \rangle$ have an approximately linear relation to $\langle T'_s \rangle$, with superimposition of nonlinear terms such as transport anomalies and contributions to evaporation anomalies by variations of wind speed. Because these tend not to be simply related to SST, they produce scatter in the relationship to $\langle T'_s \rangle$. The proportionality constant of $\langle \hat{T}' \rangle$ to $\langle T'_s \rangle$ is approximately $1.4 CC^{-1}$, which is close to what is shown in Fig. 1a. The dependence of tropical mean precipitation on $\langle T'_s \rangle$ results from competing effects of column radiative cooling and surface emissive warming. The current choice of parameters yields a rate of $0.09 \text{ mm day}^{-1}C^{-1}$. However, it is possible to have a negative slope of $\langle P' \rangle$ versus $\langle T'_s \rangle$ if the value of n varies. For example, n is generally higher when a larger area of non-precipitation regions is involved. This could result in a negative tropical mean precipitation anomaly for a given positive SST anomaly.

Most importantly, the transport anomaly terms in (7) play a greater role in producing scatter in $\langle P' \rangle$ compared to the $\langle T'_s \rangle$ term than occurs in (6) for $\langle \hat{T}' \rangle$. Contributing to this, (i) F_T' and F_q' tend to cancel in (6), and (ii) the $\langle T'_s \rangle$ term in (7) is multiplied by a small time scale, $(\epsilon_T - n\epsilon_{T_s})$.

3.3. The simplest case

Let us consider a simple case in which only evaporation is taken into account as the dominant driving force for the tropical atmospheric response to $\langle T'_s \rangle$, and sensible heat and radiative flux anomalies are neglected. In this case, setting ϵ_{T_s} and ϵ_T to zero in (6) and (7) yields

$$\langle \hat{T}' \rangle \approx \frac{\langle T'_s \rangle}{n} - (F_T' - F_q' - \langle \tilde{E} \rangle)(\epsilon_H \gamma n)^{-1} \quad (8)$$

$$\langle P' \rangle \approx F_T'. \quad (9)$$

Equivalently, (9) can be derived directly from (3.1), neglecting F_{rad}' and H' , and using $F_T' \equiv \langle D_T' \rangle$. This simply states that convective heating balances dry static energy transport. Here, the tropical mean precipitation anomalies are dominated by the midlatitude-tropical dry static energy transport anomalies and are not necessarily related to SST changes, while the tropospheric temperature anomalies still approximately linearly follow the SST anomalies. The scale factor n^{-1} gives the slope of $\langle \hat{T}' \rangle$ to $\langle T'_s \rangle$, approximately 1.73, close to the slope of the linear fit for the NSIPP ensemble simulations.

Given (9), the moisture equation (2) then implies that evaporation must balance the precipitation minus moisture transport, i.e., $\langle E' \rangle = F_T' - F_q'$. We note that this implies $\langle E' \rangle$ should be poorly related to $\langle T'_s \rangle$ on these time scales as well. (Robertson et al. 2004, personal communication).

3.4. Testing of the dominant balance for $\langle P' \rangle$

According to (9), the dry static energy transport anomaly between the tropics and mid-latitudes is a dominant factor in determining tropical mean precipitation variability. Since heat and moisture budgets tend not to be well closed in data such as the NCEP/NCAR reanalysis (Trenberth and Guillemot 1998; Su and Neelin 2002), SN03 computed the dry static energy and moisture transport anomalies for one of the NSIPP ensemble experiments. This tests the extent to which (9) gives the dominant balance for interannual $\langle P' \rangle$ variations in this model. Figure 5 shows the scatterplot of $\langle P' \rangle$ against F_T' , both in units of W m^{-2} . The tropical mean precipitation anomalies follow the dry static energy transport anomalies, with a correlation coefficient of 0.8. The linear regression gives a slope of 0.74, somewhat less than the slope of 1 predicted by the simplest case (9). The more general case, (7), gives a slope of $(1 + \epsilon_T(\epsilon_H \gamma n)^{-1})^{-1} \approx 0.6$ for the parameters given above. The slight scatter in Fig. 5 about the F_T' regression line would be due to other terms in (7). This confirms that variations of tropics-midlatitude transports can indeed play an important role in the variability of tropical mean precipitation anomalies. This holds for 3-month averages, as are shown here. At much longer time scales, the variations explained by random fluctuations of the transports would be smaller.

SN03 also verified that F_T' is not closely related to $\langle T_s' \rangle$, as the correlation coefficient between the two is only -0.1 . Our claim that $F_T' - F_q'$ has a smaller effect in producing scatter in $\langle \hat{T}' \rangle$ than F_T' does in $\langle P' \rangle$ was also verified in SN03 by examining the standard deviations associated with each term.

4. DYNAMICS BEHIND THE $\langle T' \rangle$, $\langle P' \rangle$ AND $\langle T_s' \rangle$ RELATIONS

Considering the analytical explorations in section (3.1), one notices that convective heating anomalies (\hat{Q}'_c) do not appear explicitly in the moist static energy equation (5). Does this mean that convection is not important for the tropospheric temperature response to SST? The answer is that convection is essential but the convective heating is a by-product. SN03 used a simple convective adjustment scheme and associated fast time scale τ_c to illustrate that the amount of convective heating is not relevant to the tropospheric temperature anomalies because of the small value of τ_c . In this case, tropospheric temperature is held close to a convective quasi-equilibrium (QE) profile whose variations depend primarily on boundary layer moist static energy. Departures from QE are only on the order of τ_c , regardless of the value of the heating. Convection itself is an important player in communicating between boundary layer forcing and deep tropospheric temperature re-

sponse, but the amount of convective heating is subject to the balance with various cooling terms in the temperature equation. On the tropical average, the dominant cooling term is dry static energy transport anomaly because sensible heat and radiative fluxes are associated with relatively small damping rates. The dry static energy transport, which has a large contribution from mid-latitude transients and correlates poorly with tropical SST anomalies, is thus able to create large scatter in the tropical mean precipitation anomalies with respect to SST anomalies.

Figure 6 illustrates a schematic for the dynamical processes involved in the tropical tropospheric response to SST forcing. Different arrows are used to indicate these processes, with associated time scales marked in parentheses. The short open arrow within the boundary layer indicates evaporation anomalies (E'). During an El Niño, warm SST anomalies increase evaporation, and to a lesser extent, sensible heat fluxes and radiative emission into the atmosphere. Consequently, boundary layer moist static energy h'_b is increased. The time scale associated with the boundary layer adjustment is relatively fast, as represented by the parameter $(\epsilon_H \gamma)^{-1}$. Positive h'_b would tend to yield a larger convective available potential energy (CAPE) for the atmospheric column. Stronger convection occurs over the warm water, indicated by the long solid arrow. It constrains the tropospheric temperature to a value in equilibrium with boundary layer moist static energy. The convective adjustment time scale τ_c is less than a day (Bretherton et al. 2003). Because convection establishes the equilibrium on a fast time scale, the amount of convective heating does not explicitly determine the tropospheric temperature anomaly. Across the tropics, the tropospheric temperature warming is spread horizontally by wave dynamics, as indicated in the upper plane by two horizontal arrows pointing outwards from the origin of the warming and by gray shading representing the propagating warm anomalies. The corresponding time scale results from a combination of tropical moist and dry Kelvin or Rossby waves propagating across the domain, with phase speeds on the order of 10–50 m s^{-1} . For the tropical band, this yields a time scale of 1–2 weeks to 1–2 months. The wave dynamics does not show up explicitly in our analysis for tropical averages, but is important to the large-scale features of the temperature anomalies. Hence, the tropospheric temperature anomalies are wide-spread and its tropical average is approximately linear with tropical mean SST anomalies. Nonlinearity due to the mid-latitudes transports and the dependence of fluxes on the $\langle T'_s \rangle$ and $\langle \hat{T}' \rangle$ are weak because of the predominance of approximate linear boundary layer flux adjustment. The curly dashed arrows in Fig. 6 indicate radiative cooling associated with tropospheric temperature anomalies. It is a

relatively slow damping process with a characteristic time scale of 15 days, proportional to ϵ_T^{-1} .

Associated with the warming of tropospheric temperature across the tropics, the CAPE tends to decrease in regions away from the warm SST anomaly, unless atmospheric boundary layer (ABL) moist static energy is able to compensate. Reduction of precipitation thus tends to occur, as shown in Fig. 6 by the shorter solid arrow with less dense rainfall. The mechanisms for the relative subsidence involve complicated pathways (Su and Neelin 2002). Anomalous moisture or temperature advection, evaporation anomalies due to changes in surface wind speed or air-sea moisture differences and changes in gross moist stability due to moisture variations, etc, can all come into play to balance the adiabatic warming associated with the relative descent. On the tropical average, the dry static energy transport anomalies, F_T' , appear to be an important constraint for precipitation anomalies. Suppose there is net dry static energy export from the tropics to the midlatitude, as indicated by the dark slanted arrow in Fig. 6. It produces a cooling tendency in the dry static energy equation. Thus the tropical mean convective heating anomalies have to be positive to compensate the cooling effect. This fits in the “normal” picture that tropical mean precipitation anomalies increase as tropical SST warms during an El Niño. On the other hand, dry static energy transport anomalies between the tropics and mid-latitude are presumably substantially due to midlatitude transient eddy activity. The F_T' can be negative (import into the tropics) even during warm SST years. In this case, the warming effect caused by dry static energy import would tend to reduce CAPE and suppress convection over climatologically convecting regions. This could result in negative precipitation anomalies on the tropical average, which seems counter-intuitive.

The dry static energy transport anomalies F_T' can have contributions from atmospheric internal variability, and contributions associated with the response to SST anomalies. In the latter case, the precipitation scatter persists even in an ensemble average over many atmospheric model runs, as seen in Fig. 4b. The important factor in the scatter is that the tropics to midlatitude dry static energy transport is not closely related to tropical average SST anomalies. Nonlinearity in the transport response to SST can thus play a role.

Because the dry static energy transport anomalies bear no simple relation to tropical SST anomalies, the tropical mean precipitation anomalies are scattered in relation to SST. For the tropospheric temperature anomalies, the magnitude of moist static energy transport anomalies is much smaller than that of the forcing from the boundary layer, thus the scatter of $\langle \hat{T}' \rangle$ is small. For tropical mean precipitation anomalies, the dry static energy transport anomalies are competing against relatively small damping rates associated with radiation, and

thus transport anomalies are able to create large scatter in $\langle P' \rangle$ in relation to $\langle T'_s \rangle$.

5. CONCLUSION AND DISCUSSION

On interannual time scales, there are substantial tropospheric temperature and precipitation anomalies associated with the variations of tropical SST. The spatial pattern of tropospheric temperature response tends to be smooth and wide-spread because of the effectiveness of wave dynamics in spreading the temperature anomalies. Because the spatial extent of the temperature response is large even when the SST forcing is highly localized, the tropical mean tropospheric temperature anomaly $\langle \hat{T}' \rangle$ is highly relevant as a measure of the dynamical response, in addition to being of interest in global warming related studies. It bears an approximately linear relationship to tropical mean SST anomalies. On the other hand, tropical precipitation response to ENSO SST tends to be highly non-uniform in spatial pattern. Positive precipitation anomalies are local to warm SST anomalies. Strong negative precipitation anomalies tend to occur within the convective zones and relatively near the positive SST anomalies, while weaker negative precipitation anomalies occur in the far-field. The near-cancellation of positive and negative precipitation anomalies produces a scattered tropical mean precipitation anomalies in relation to tropical mean SST anomalies. For this reason, the *tropical mean precipitation anomaly* $\langle P' \rangle$ is a poor measure of tropical hydrological cycle on interannual time scales.

The dynamics governing the different relationships between $\langle \hat{T}' \rangle$ and $\langle T'_s \rangle$ and between $\langle P' \rangle$ and $\langle T'_s \rangle$ are examined using a simple analytical model. This suggests that the scatter of $\langle P' \rangle$ against $\langle T'_s \rangle$ is associated with dry static energy transport anomalies between the tropics and mid-latitudes, changes in evaporation due to wind speed variations and other nonlinear effects. In contrast, the effects of anomalous midlatitude-tropical transports and nonlinearities are secondary on the $\langle \hat{T}' \rangle$ relation to $\langle T'_s \rangle$ because of the strong linkage between SST, boundary layer moist static energy, and tropospheric temperature through boundary layer flux adjustment and tropospheric convective adjustment.

Following the convective quasi-equilibrium point of view (Arakawa and Schubert 1974; Emanuel et al. 1994), the linear relationship between the tropical averaged tropospheric temperature and SST regardless of the value of tropical mean precipitation is not surprising. Convection establishes a link between tropospheric temperature and ABL moist static energy, which in turn is constrained toward SST by surface fluxes. The convective heating anomaly itself is simply a by-product that can be positive or negative depending on other terms in the temperature equation, such as random variations in midlatitude-tropical transports. When convection commu-

nicates boundary layer anomalies upward to constrain tropospheric temperature, the convective heating anomaly must react to oppose any process that would tend to cool or warm the troposphere away from balance with SST. We note that the relationship found in this study holds on interannual time scales. On shorter time scales and smaller spatial scales, QE constrain is less strictly satisfied (Brown and Bretherton 1997; Sobel et al. 2003). For cases at longer time scales and global spatial scales, such as global warming or paleoclimate applications, it is possible that the dominant cooling effects (for example, the radiative effects) have a rather simple relationship to tropospheric temperature, which in turn would produce a simple precipitation and SST relationship. For the interannual variations examined here, the dominant anomalous cooling process on the tropical average is the tropics-to-midlatitude dry static energy transport anomalies, which have little relationship to SST. Hence there is large scatter in tropical mean precipitation anomalies in relation to SST due to the midlatitude dry static energy transport variations.

The approximately linear relationship of $\langle \hat{T}' \rangle$ with $\langle T'_s \rangle$ and scattered $\langle P' \rangle$ with $\langle T'_s \rangle$ are results of the combined effects of quasi-equilibrium convective adjustment processes and midlatitude-tropical transports. The contrasting behavior of tropical mean tropospheric temperature and precipitation in relation to SST is a nice illustration of the usefulness of convective QE approaches to understanding the interaction of tropical convection with large-scale dynamics.

Acknowledgments. This work was supported under National Science Foundation Grant ATM-0082529, National Oceanographic and Atmospheric Administration Grant NA16-GP2003 and National Aeronautics and Space Administration Grant NA-GS-9358. The authors thank I. Held, A. H. Sobel, C. S. Bretherton, and M. P. Hoerling for discussions.

REFERENCES

- Angell, J. K., Comparison of variations in atmospheric quantities with sea surface temperature variations in the equatorial eastern Pacific. *Mon. Wea. Rev.*, 109, 230-243, 1981.
- Arakawa, A. and W. H. Schubert, Interaction of a cumulus cloud ensemble with the large-scale environment, Part I. *J. Atmos. Sci.*, 31, 674-701, 1974.
- Bacmeister, J., P. J. Pegion, S. D. Schubert, and M. J. Suarez, Atlas of Seasonal Means Simulated by the NSIPP 1 Atmospheric GCM, *NASA/TM-2000-104505*, volume 17, 2000.
- Bretherton, C. S., M. E. Peters, and L. E. Back, Relationships between water vapor path and precipitation over the tropical oceans. *J. Climate*, submitted, 2003

- Dai, A., T. M. L. Wigley, B. A. Boville, J. T. Kiehl, and L. E. Buja, Climates of the twentieth and twenty-first centuries simulated by the NCAR climate system model. *J. Climate*, *14*, 485-519, 2001.
- Emanuel, K. A., J. D. Neelin and C. S. Bretherton, On large-scale circulations in convecting atmospheres. *Quart. J. Roy. Meteor. Soc.*, *120*, 1111-1143, 1994.
- Gill, A. E., Some simple solutions for heat induced tropical circulation. *Quart. J. Roy. Meteor. Soc.*, *106*, 447-462, 1980.
- Holton, J. R., *An introduction to dynamic meteorology* (third edition), 511pp. Academic Press, San Diego, Calif., 1992.
- Horel, J. D., and J. M. Wallace, Planetary-scale atmospheric phenomena associated with the Southern Oscillation. *Mon. Wea. Rev.*, *109*, 813-829, 1981.
- Huffman, G. J. and co-authors, The Global Precipitation Climatology Project (GPCP) combined data set. *Bull. Amer. Meteor. Soc.*, *78*, 5-20, 1997.
- Kalnay, E., et al., The NCEP/NCAR 40-year reanalysis project. *Bull. Amer. Meteor. Soc.*, *77*, 437-471, 1996.
- Kiladis, G. N., and H. F. Diaz, Global climatic anomalies associated with extremes in the Southern Oscillation. *J. Climate*, *2*, 1069-1090, 1989.
- Kumar, A., and M. P. Hoerling, The nature and causes for the delayed atmospheric response to El Niño. *J. Climate*, *16*, 1391-1403, 2003.
- Mitchell, J. F. B., C. A. Wilson, and W. M. Cunningham, On CO₂ climate sensitivity and model dependence of results. *Quart. J. Roy. Meteor. Soc.*, *113*, 293-332, 1987.
- Neelin, J. D., and N. Zeng, A quasi-equilibrium tropical circulation model—formulation. *J. Atmos. Sci.*, *57*, 1741-1766, 2000.
- Newell, R. E., and B. C. Weare, Ocean temperatures and large scale atmospheric variations. *Nature*, *262*, 40-41, 1976.
- Pan, Y. H., and A. H. Oort, Global climate variations connected with sea surface temperature anomalies in the eastern equatorial Pacific Ocean for the 1958-73 Period. *Mon. Wea. Rev.*, *111*, 1244-1258, 1983.
- Pegion, P. J., S.D. Schubert, and M.J. Suarez, An Assessment of the Predictability of Northern Winter Seasonal Means with the NSIPP 1 AGCM, *NASA/TM-2000-104505*, volume 18, 2000.
- Reynolds, R. W., and T. M. Smith, Improved global sea surface temperature analyses using optimum interpolation, *J. Climate*, *7*, 929-948, 1994.
- Ropelewski, C. F. and M. S. Halpert, Global and regional scale precipitation associated with El Niño/Southern Oscillation, *Mon. Wea. Rev.*, *115*, 1606-1626, 1987.
- Spencer, R. W., Global oceanic precipitation from the MSU during 1979-91 and comparisons to other climatologies. *J. Climate*, *6*, 1301-1326, 1993.

- Spencer, R. W., and J. R. Christy, Precision and Radiosonde Validation of Satellite Grid-point Temperature Anomalies. Part II: A Tropospheric Retrieval and Trends during 1979–90. *J. Climate*, 5, 858–866, 1992.
- Sobel, A. H., I. M. Held, and C. S. Bretherton, The ENSO signal in tropical tropospheric temperature. *J. Climate*, 15, 2702–2706, 2002.
- Sobel, A. H., S. E. Yuter, C. S. Bretherton, and G. N. Kiladis, Large-scale meteorology and deep convection during TRMM KWAJEX. *Mon. Wea. Rev.*, accepted, 2003.
- Soden, B. J., The sensitivity of the tropical hydrological cycle to ENSO. *J. Climate*, 13, 538–549, 2000.
- Su, H., J. D. Neelin, and C. Chou, Tropical teleconnection and local response to SST anomalies during the 1997–1998 El Niño. *J. Geophys. Res.*, 106, 20,025–20,043, 2001.
- Su, H., and J. D. Neelin, Teleconnection mechanisms for tropical Pacific descent anomalies during El Niño. *J. Atmos. Sci.*, 59, 2682–2700, 2002.
- Su, H., J. D. Neelin, and J. E. Meyerson, Sensitivity of tropical tropospheric temperature to sea surface temperature forcing. *J. Climate*, 16, 1283–1301, 2003.
- Su, H., and J. D. Neelin, The scatter in tropical average precipitation anomalies. *J. Climate*, in press, 2003.
- Sun, D. Z., and A. H. Oort, Humidity-temperature relationships in the tropical troposphere. *J. Climate*, 8, 1974–1987, 1995.
- Trenberth, K. E., and C. J. Guillemot, Evaluation of the atmospheric moisture and hydrological cycle in the NCEP/NCAR reanalysis, *Climate Dynamics*, 14, 213–231, 1998.
- Wallace, J. M., E. M. Rasmusson, T. P. Mitchell, V. E. Kousky, E. S. Sarachik and H. von Storch, On the structure and evolution of ENSO-related climate variability in the tropical Pacific: Lessons from TOGA, *J. Geophys. Res.*, 103, 14241–14260, 1998.
- Xie, P., and P. A. Arkin, Global precipitation: A 17-year monthly analysis based on gauge observations, satellite estimates and numerical model outputs, *Bull. Amer. Meteor. Soc.*, 78, 2539–2558, 1997.
- Yulaeva, E. and J. M. Wallace, The signature of ENSO in global temperature and precipitation fields derived from the microwave sounding unit, *J. Climate*, 7, 1719–1736, 1994.
- Zeng, N., J. D. Neelin, and C. Chou, A quasi-equilibrium tropical circulation model—implementation and simulation. *J. Atmos. Sci.*, 57, 1767–1796, 2000.

J. E. Meyerson, H. Su, J. D. Neelin, Department of Atmospheric Sciences, University of California, Los Angeles, Los Angeles, CA 90095-1565, (e-mail: hui@atmos.ucla.edu; neelin@atmos.ucla.edu; hobo@atmos.ucla.edu)

Figure 1.1. Tropical averaged (25S-25N) (a) tropospheric temperature and (b) precipitation anomalies versus tropical averaged SST anomalies for various datasets (see text for details, Fig. 1a. modified after SNM Fig. 1) The solid lines are the linear fits to the datasets (the NCEP and GPCP precipitation have the same linear fits). The slopes of the linear fits are listed by the values of m .

Figure 1.1. Tropical averaged (25S-25N) (a) tropospheric temperature and (b) precipitation anomalies versus tropical averaged SST anomalies for various datasets (see text for details, Fig. 1a. modified after SNM Fig. 1) The solid lines are the linear fits to the datasets (the NCEP and GPCP precipitation have the same linear fits). The slopes of the linear fits are listed by the values of m .

Figure 1.2. Spatial patterns of precipitation anomalies from the GPCP data for (a) September to November 1997 and (b) for December 1997 - January 1998. After SN03 (their Figs. 2b and 3b).

Figure 1.2. Spatial patterns of precipitation anomalies from the GPCP data for (a) September to November 1997 and (b) for December 1997 - January 1998. After SN03 (their Figs. 2b and 3b).

Figure 1.3. Scatterplot of tropical mean (25S-25N) (a) precipitation anomalies (in mm day^{-1}) and (b) tropospheric temperature (850-200 mb) anomalies (in C) as a function of tropical average SST anomalies (in C) from 1982 to 1998 for the five NSIPP AGCM ensemble simulations. Corresponding least-square linear fits are shown by dashed lines, with slopes marked (units of $\text{mm day}^{-1} \text{C}^{-1}$ and unitless, respectively). From SN03 (their Fig. 6).

Figure 1.3. Scatterplot of tropical mean (25S-25N) (a) precipitation anomalies (in mm day^{-1}) and (b) tropospheric temperature (850-200 mb) anomalies (in C) as a function of tropical average SST anomalies (in C) from 1982 to 1998 for the five NSIPP AGCM ensemble simulations. Corresponding least-square linear fits are shown by dashed lines, with slopes marked (units of $\text{mm day}^{-1} \text{C}^{-1}$ and unitless, respectively). From SN03 (their Fig. 6).

Figure 1.4. (a) Tropical averaged (25S-25N) tropospheric temperature anomalies versus the spatial integral of SST anomaly forcing for a number of experiments with subregions of the 1998 JFM El Niño SST anomaly. The side-panels show examples of the simulated tropospheric temperature anomalies, with heavy outlines indicated the regional SST forcings used. (b) Tropical averaged (25S-25N) precipitation anomalies versus the spatial integral of SST anomaly forcing for the same experiments as in (a). The side-panels show examples of the spatial distribution of precipitation anomalies for runs in Fig. 4a side panels. Modified after SNM (their Figs. 6b, 8b, 9b and 10, plus one case not shown in SNM).

Figure 1.4. (a) Tropical averaged (25S-25N) tropospheric temperature anomalies versus the spatial integral of SST anomaly forcing for a number of experiments with subregions of the 1998 JFM El Niño SST anomaly. The side-panels show examples of the simulated tropospheric temperature anomalies, with heavy outlines indicated the regional SST forcings used. (b) Tropical averaged (25S-25N) precipitation anomalies versus the spatial integral of SST anomaly forcing for the same experiments as in (a). The side-panels show examples of the spatial distribution of precipitation anomalies for runs in Fig. 4a side panels. Modified after SNM (their Figs. 6b, 8b, 9b and 10, plus one case not shown in SNM).

Figure 1.5. Scatterplot of tropical mean (25S-25N) precipitation anomalies (in $W m^{-2}$) as a function of the anomalies in the export of dry static energy from the tropics by atmospheric dynamical transports across 25 S and 25 N (in $W m^{-2}$). The results are from 1982 to 1998 for one of the NSIPP AGCM simulations. Corresponding least-square linear fit is shown by the dashed line, with its slope marked. From SN03 (their Fig. 7).

Figure 1.5. Scatterplot of tropical mean (25S-25N) precipitation anomalies (in $W m^{-2}$) as a function of the anomalies in the export of dry static energy from the tropics by atmospheric dynamical transports across 25 S and 25 N (in $W m^{-2}$). The results are from 1982 to 1998 for one of the NSIPP AGCM simulations. Corresponding least-square linear fit is shown by the dashed line, with its slope marked. From SN03 (their Fig. 7).

Figure 1.6. Schematic of the dynamic processes involved in the tropical tropospheric temperature and precipitation response to SST forcing. After SN03 (their Fig. 8).

Figure 1.6. Schematic of the dynamic processes involved in the tropical tropospheric temperature and precipitation response to SST forcing. After SN03 (their Fig. 8).

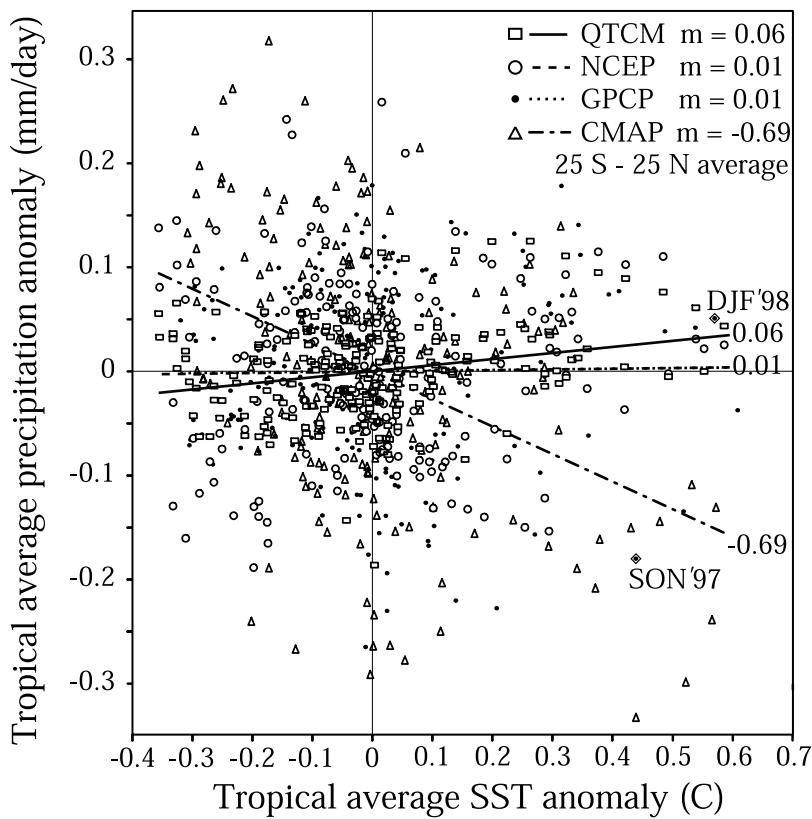
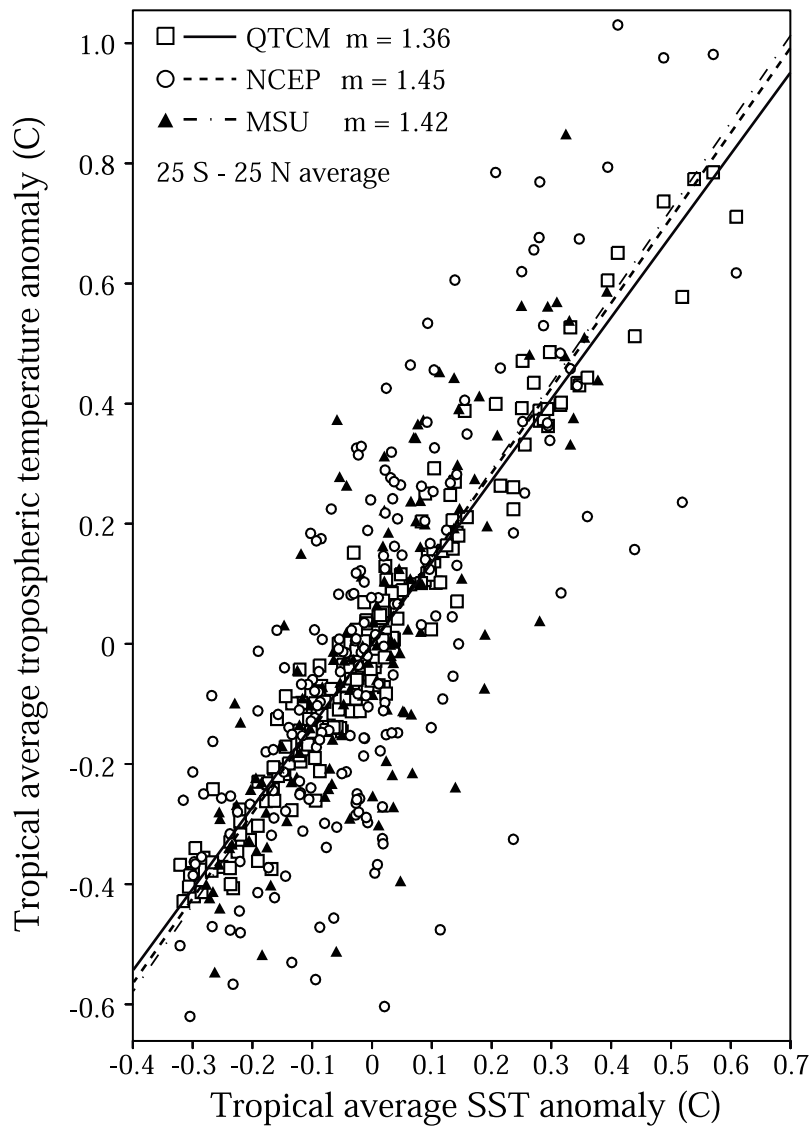


Figure 1

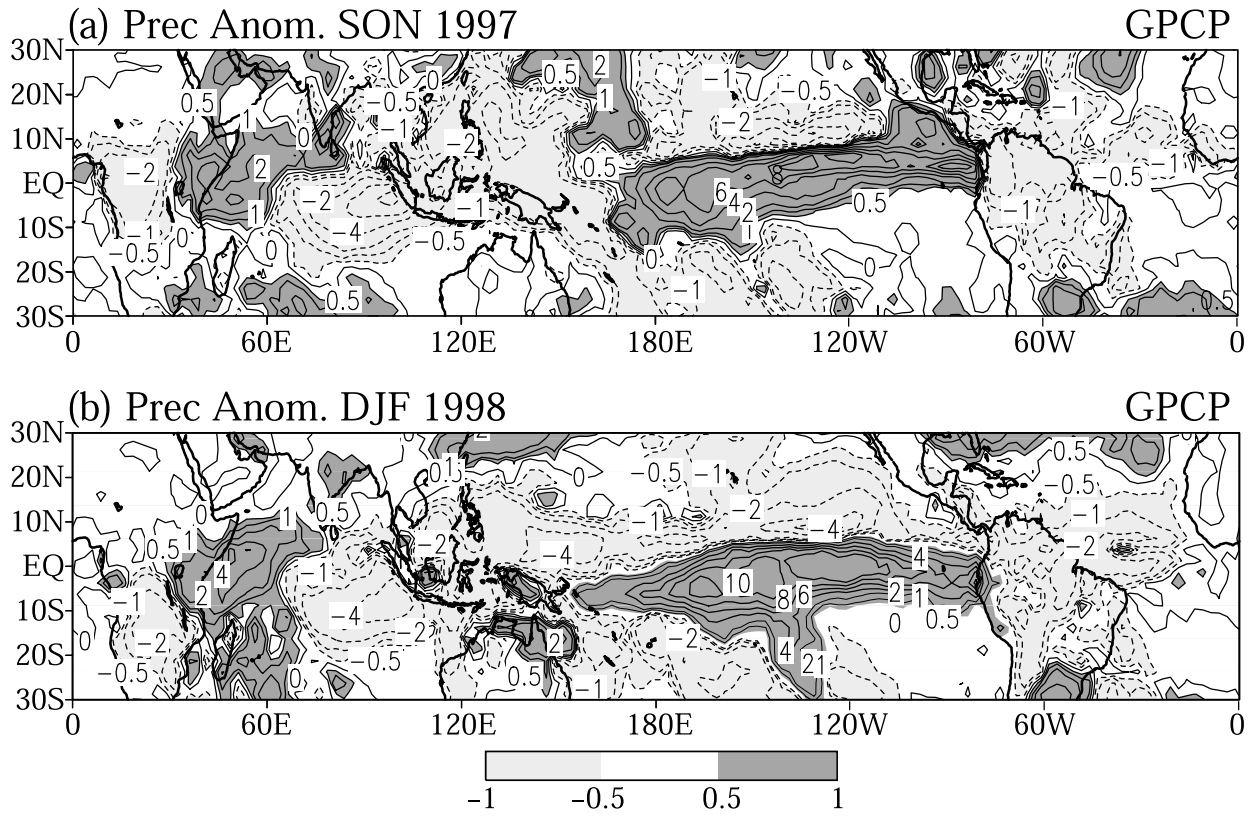


Figure 2

5 NSIPP AGCM Experiments 1982 - 1998
(3 month mean)

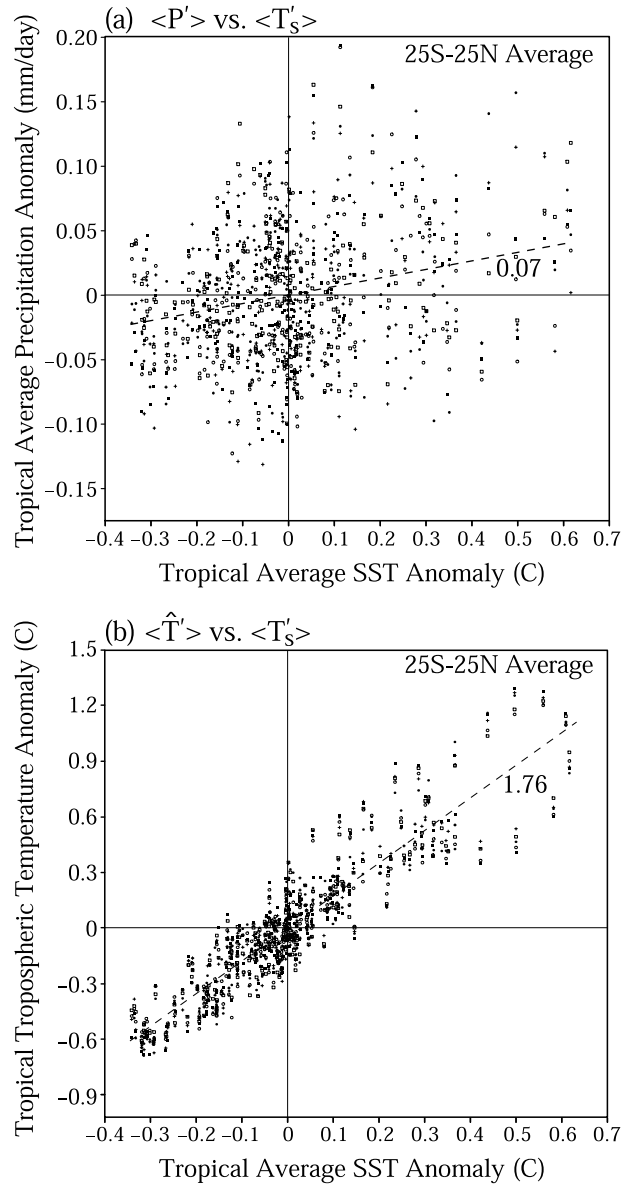


Figure 3

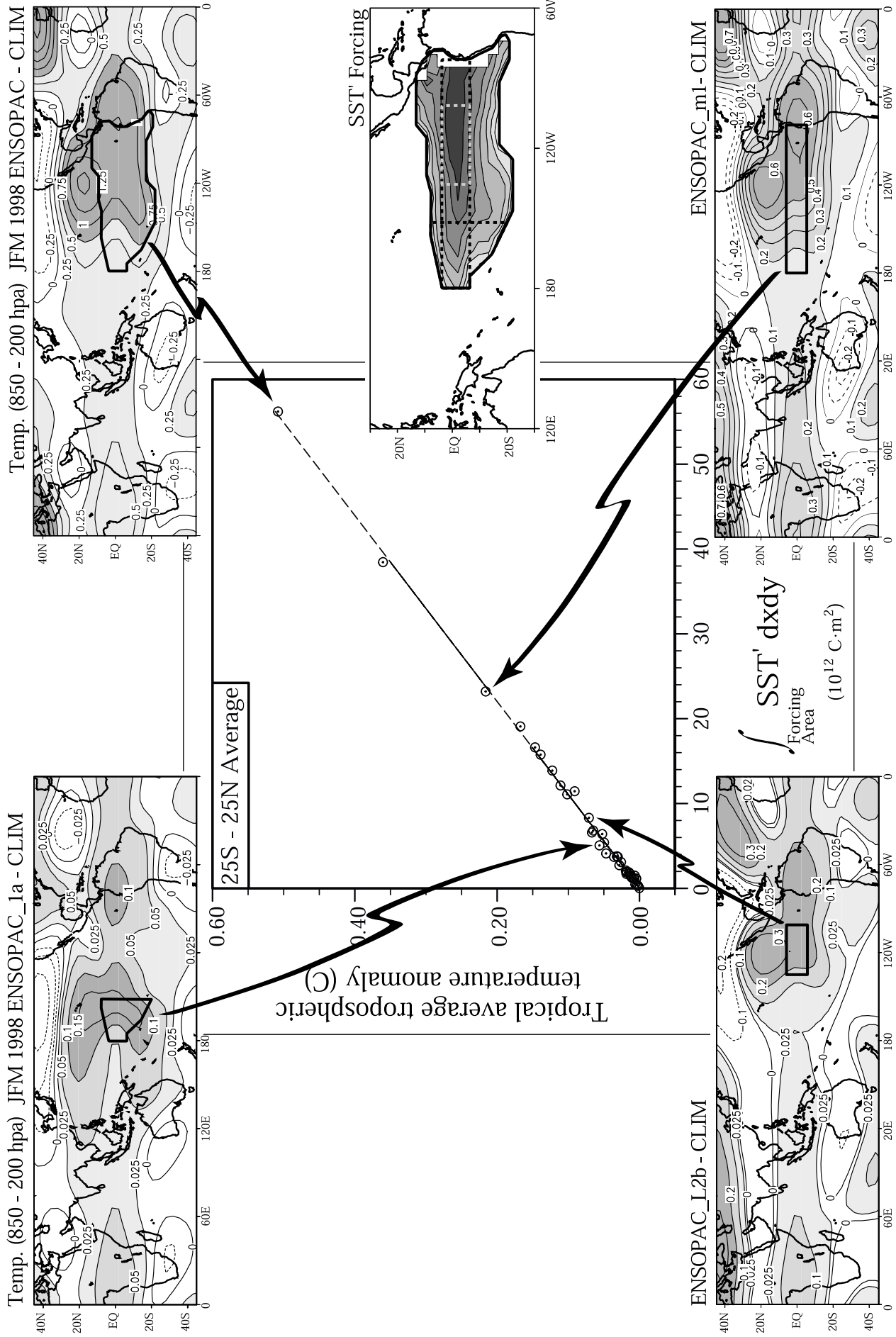


Figure 4a

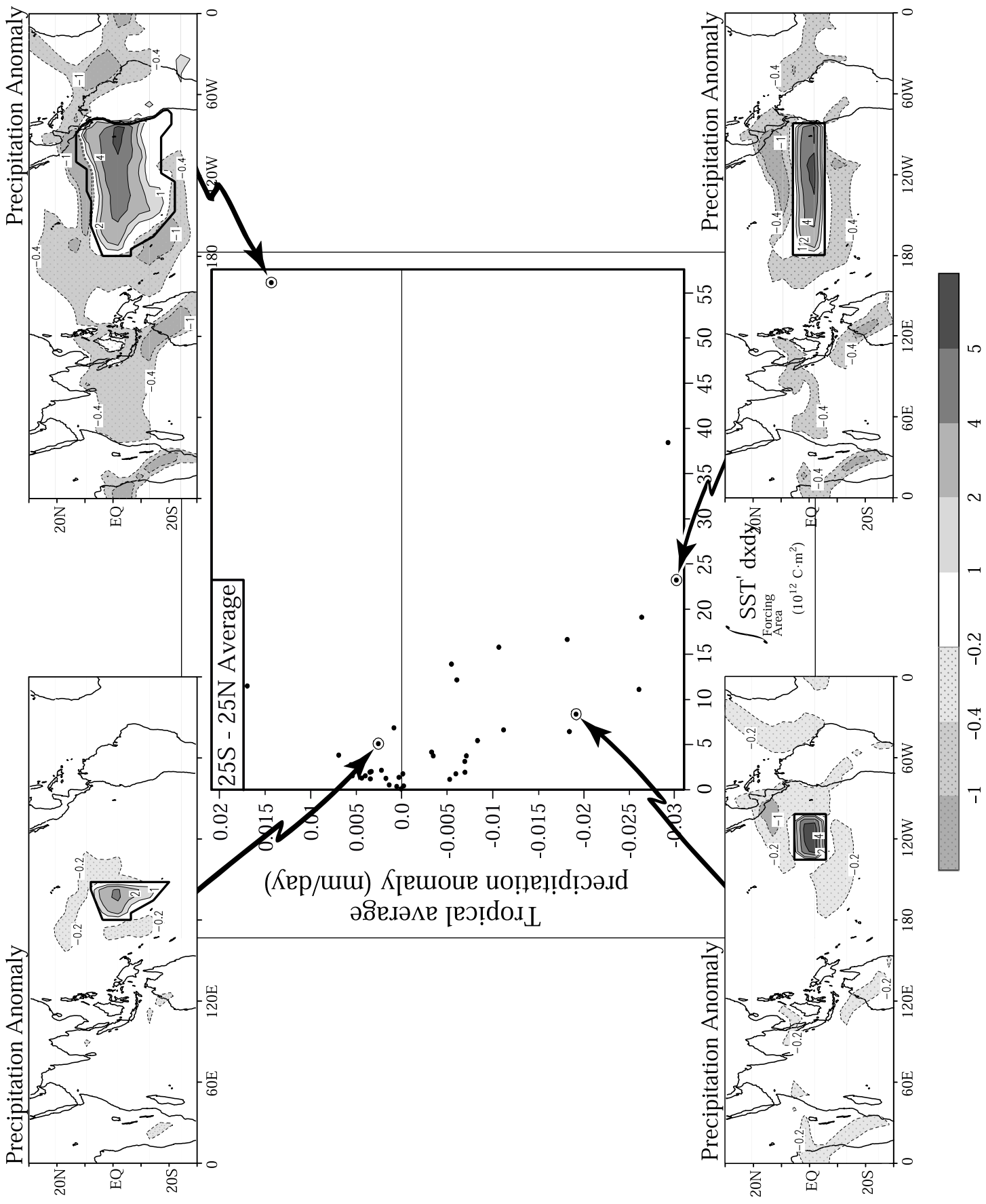


Figure 4b

1 NSIPP AGCM Experiment 1982 - 1998
(3 month mean)

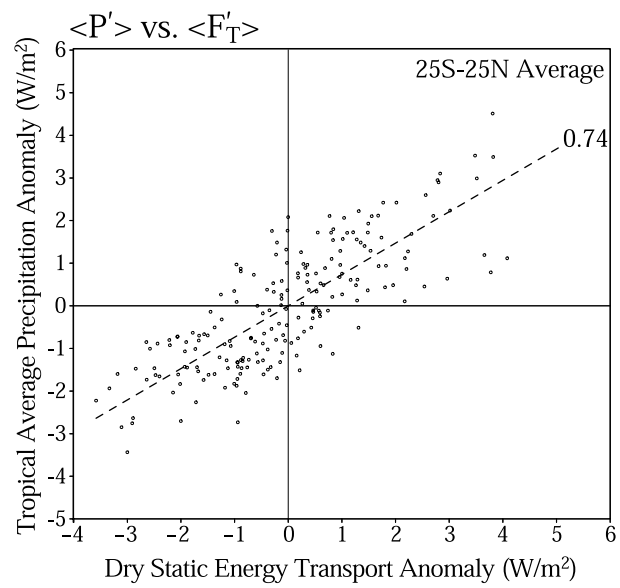


Figure 5

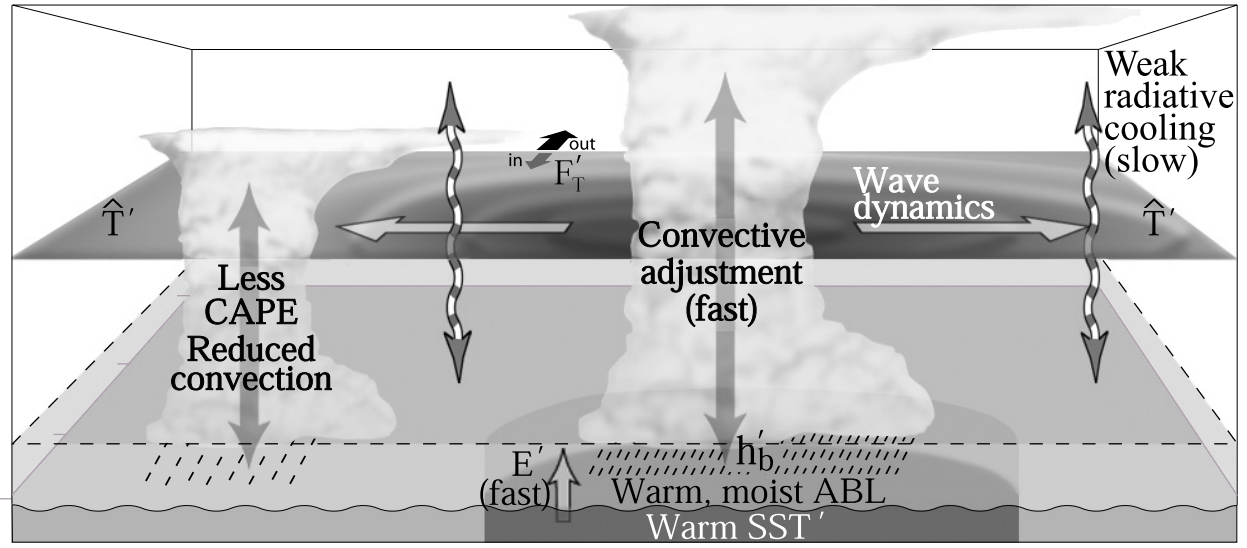


Figure 6